Astron. Astrophys. 297, 861–868 (1995)

ASTRONOMY AND ASTROPHYSICS

The Eversheld effect: rise and fall of the wave model

M. Bünte and S.K. Solanki

Institut für Astronomie, ETH Zentrum, CH–8092 Zürich, Switzerland

Received 31 March 1994 / Accepted 22 October 1994

Abstract. Adiabatic surface and trapped body waves have recently been proposed as the source of the Evershed effect. We show that such waves fail to simultaneously reproduce the main features of the Evershed effect in a set of spectral lines with different temperature sensitivities. This result sets constraints on all models that attempt to explain the Evershed effect on the basis of a wave-like correlation between temperature and velocity. In the photospheric layers in which the waves are expected to propagate, dissipative effects due to radiative diffusion are likely to damp the wave-induced temperature perturbations. We show, however, that in the line forming penumbral layers radiatively damped ("isothermal") waves shift spectral lines of neutral and ionized species in opposite directions. We conclude that, in spite of a number of highly attractive features, linear wave models have great difficulty in explaining the Evershed effect.

Key words: sunspots – MHD – radiative transfer – line: profiles

1. Introduction

It has been shown recently that magneto-atmospheric surface and trapped body waves propagating parallel to the interface between a sunspot penumbra and the underlying convection zone can produce spectral line shifts and asymmetries (Bünte et al. 1993) that are in good agreement with observations of the well known Evershed phenomenon (Evershed 1909; Schröter 1965; Stellmacher & Wiehr 1980; Schröter et al. 1989).

These surface waves are restricted to magnetic interfaces and hence should mostly be present in the penumbra but absent in the umbra. Their spatial decay away from the interface is in good agreement with the observed decrease of the Evershed shifts with height, and since waves do not transport any mass, they resolve the problem of mass conservation at the outer penumbral boundary which is proposed by recent observations (Solanki et al. 1992, 1994). Furthermore, since the temperature perturbations are in phase with the horizontal, but 90° out of phase with the vertical velocity component, this wave model can account for the fact that the Evershed signature is visible only in observations close to the solar limb and vanishes at disc centre. Thus surface waves possess many features which make them an attractive mechanism for producing the spectral signature of the Evershed effect. In addition, recent high resolution observations suggest that the Evershed effect is non-stationary, and possibly wave-like in nature (Rimmele 1993; see also Lamb 1975).

While Bünte et al. (1993) concentrated on the single Fe I line at 5250.2 Å, we study in this contribution the signature of the surface wave model in a variety of spectral lines. These results have in part been summarized by Bünte (1993) and Bünte & Solanki (1994). In Sect. 2 we demonstrate that the temperature-velocity correlation of adiabatic surface waves leads to spectral line shifts and asymmetries whose sign and magnitude depend on the temperature sensitivity of the line under investigation.

In Sect. 3 we extend the surface wave model by including radiative dissipation in the Newtonian cooling approximation. In Sect. 4 we present results for magneto-atmospheric surface waves subject to strong radiative dissipation. We find that such waves lead to shifts and asymmetries of opposite sign in Fe I and Fe II lines. In contrast, the calculations of Eriksen & Maltby (1967) and Maltby & Eriksen (1967) suggest that for an isothermal wave in an unstratified atmosphere the pressure-velocity correlation affects spectral lines in a systematic way, independently of their temperature sensitivity. We discuss the influence of the pressure fluctuations on spectral lines in detail and show that it is the temperature stratification of the equilibrium atmosphere – taken explicitly into account in our radiative transfer calculations – which is responsible for the fundamental difference between the results obtained by Maltby & Eriksen and by us. A critical discussion of the model and our conclusions are presented in Sect. 5.

Before unveiling the shortcomings of the adiabatic wave model let us briefly describe the geometry and the atmospheric parameters of the current calculations. All the waves considered in the present paper propagate parallel to a horizontal interface separating an upper magnetic from a lower non-magnetic layer. We consider a horizontal field of strength 1000 G, typical for the penumbra. The atmosphere above the interface is described by the penumbral model of Ding & Fang (1989), below the interface by the convection zone model of Spruit (1977). The two layers are matched under the requirement of pressure bal-

Send offprint requests to: S.K. Solanki

ance across the interface. As a first approximation to the mode-structure of this equilibrium we compute the modes in a two-layered equilibrium with constant temperatures in each layer. This case can be solved analytically (Miles et al. 1992) and may be easily extended to account for effects due to Newtonian cooling, as demonstrated in Sect. 3. In the adiabatic case one finds two types of modes, a low-phase speed mode and several high-phase speed, trapped harmonic modes (body modes) which appear due to the exponential increase of the Alfvén speed with height (Miles et al. 1992). Further details are given by Bünte et al. (1993). The mode structure of isothermal waves in our penumbral model is described in Sect. 3.

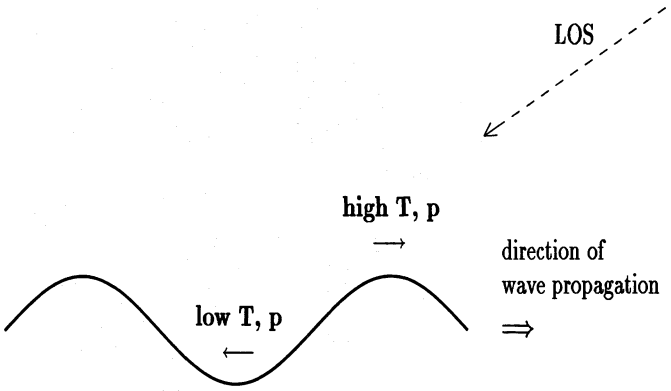

Fig. 1. Schematic drawing of an adiabatic surface wave propagating horizontally to the right. The correlated temperature, pressure, and horizontal velocity perturbations are indicated

2. The temperature-velocity correlation of adiabatic magneto-atmospheric waves

As pointed out by Darconza (1992) and Bünte et al. (1993) the correlation of the temperature perturbation with the *horizontal* velocity component leads to a net effect on spectral line profiles for observations close to the limb. In Fig. 1 this is schematically illustrated for a wave travelling to the right (i.e. towards the observer).

Above the crests of the wave the temperature and pressure are increased while in the troughs they are reduced. In an isothermal atmosphere the temperature changes are solely due to compression and expansion of the gas, i.e. $T_1 = -(\gamma - 1) T_0 \,\mathrm{div}\boldsymbol{\xi}$, where $\gamma = c_p/c_V$ is the ratio of the specific heats at constant pressure and volume, respectively, and $\boldsymbol{\xi}$ describes the wave-induced displacement of the particles. If the temperature T_0 of the equilibrium atmosphere decreases with height (as in our penumbral model) there is the additional effect of hot gas being lifted upwards into cooler regions and cool gas being pushed downwards into hotter domains, i.e. there is an additional temperature change of magnitude $-\xi_z \mathrm{d}T_0/\mathrm{d}z$. Since we solve for the wave modes in an isothermal atmosphere we neglect the latter contribution to T_1 and evaluate the wave perturbations at each height in our penumbral model as if the local temperature was constant throughout the atmosphere.

This zeroth order treatment of the temperature gradient fully accounts for the intrinsic correlations between the wave perturbations without introducing spurious qualitative changes. The temperature fluctuations obtained in this way are still considerable (up to 20 % in the line forming layers). Since the neglected term in T_1 acts in the same direction as the compressional term, the perturbations are expected to be even more pronounced in a self-consistent treatment of the wave modes.

As shown schematically in Fig. 1 for adiabatic waves the horizontal motion of the particles is correlated with the thermodynamic perturbations such that, when observing along an inclined line-of-sight (LOS, the dashed line in Fig. 1) close to the solar limb, the low-temperature regions move *away* from the observer while the high temperature regions move *towards* the observer. This correlation can lead to a net shift and/or asymmetry when averaging spatially over a full wavelength (or, equivalently, when averaging temporally over a full wave period). Due to the 90° phase shift between temperature perturbations and the *vertical* velocity component such effects vanish at disc centre. The net influence of the temperature – velocity correlation on a spectral line depends crucially on the interplay between three effects:

1. The continuum and number density enhancements associated with the high temperature domains increases their contribution to the average spectrum.
2. Temperature changes shift the ionization equilibrium by inducing fluctuations in the number densities of neutral and ionized species. This favours low temperature regions for neutrals and high temperature regions for ionized species.
3. The lower the excitation potential of a spectral line the more it is strengthened in the low temperature regions and weakened in the high-temperature regions.

For neutrals the second effect counteracts the first but cannot completely compensate it. Hence, the outcome of the averaging process depends on the third agent, the temperature sensitivity of the spectral line under consideration (due to its excitation potential), and one cannot expect to *systematically* reproduce the observed Evershed signature in lines whose excitation potentials differ significantly (cf. Eriksen & Maltby 1967).

This is demonstrated by comparing the three Fe I lines at 5250.2 Å, 5576.1 Å, and 15648.5 Å which have low (0.12 eV), medium (3.43 eV), and high (5.43 eV) excitation potentials and consequently high, intermediate, and low temperature sensitivities, respectively.

In Fig. 2 we have plotted the spectral line profiles arising from the two-layered penumbral model, perturbed by the first harmonic surface mode with a wavelength of $\lambda_x = 700$ km (corresponding to a period of 90 s) and a vertical velocity amplitude of 0.75 km s^{-1}. For a LOS inclined by 70° to the surface normal (i.e. $\theta = 70°$), this yields a maximum LOS-velocity of 1.24 km s^{-1}. The calculation corresponds to the observation of either the limb- or the centre-side penumbra of a sunspot (at $\mu = 0.34$ on the solar disc) in which one particular direction of

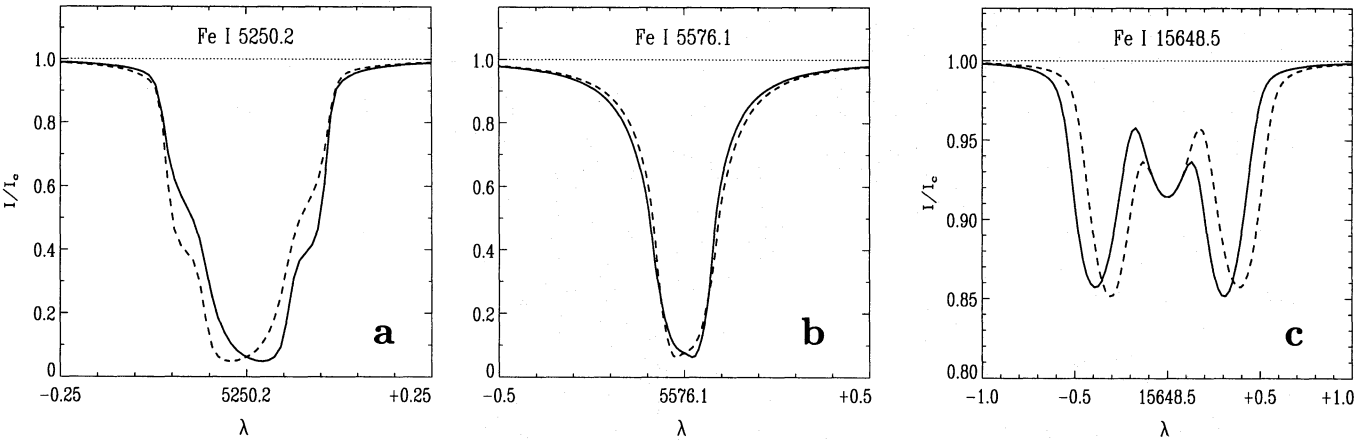

Fig. 2a–c. Line profiles of **a** Fe I 5250.2 Å, **b** 5576.1 Å, and **c** 15648.5 Å synthesized in the presence of the adiabatic ($\tau_R = +\infty$) fast mode ($\lambda_x = 700$ km, $P = 90$ s; $\hat{v}_{1z}(0) = 0.75$ km s^{-1}) close to the limb ($\theta = 70°$; solid). The dashed lines represent the mirrored line profile in each case. The profiles show shifts and asymmetries of different signs due to their different temperature sensitivities. In contrast, at disc centre they are symmetric

wave propagation, parallel or anti-parallel to the magnetic field lines, prevails[1].

To visualize the shift and asymmetry of each line we have also plotted the mirrored profile in each case (dashed lines). At disc centre, $\theta = 0°$, the profiles are strictly symmetric. For the temperature sensitive line at 5250.2 Å (Fig. 2a) the changes in line strength, i.e. the trough contributions, dominate over the changes in continuum intensity, giving rise to a net *red*-shift of the line profile. In contrast, the averaged spectrum of the temperature insensitive infrared line (Fig. 2c) is dominated by the continuum enhancement in the high-temperature domains (the crests) and hence shows a net *blue*-shift. In the case of the line at 5576.1 Å (Fig. 2b) with intermediate temperature sensitivity, the above three effects approximately cancel.

While in this model the theoretical line shifts depend obviously on line properties the observed shifts merely depend on whether limb- or centre-side penumbra is considered – independent of spectral line properties. Hence, the *adiabatic* surface wave model cannot account for this crucial observational characteristic of the Evershed effect. Since the evil arises from the temperature perturbations induced by the waves, it is worth reconsidering the assumption of adiabaticity in a radiatively dominated atmospheric layer such as the photosphere.

3. Radiating magneto-atmospheric waves

The layers in which the waves have their largest amplitudes (the photosphere) are dominated by radiative energy transport and, hence, it is to be expected that also the wave-induced temperature perturbations are subject to radiative damping.

[1] The un-identified excitation mechanism, e.g. granulation, may lead to waves which propagate radially outwards or inwards from the umbra.

3.1. Newtonian cooling

To account for radiative energy exchange the magneto-hydrodynamic (MHD) equations must in principle be solved simultaneously with the radiative transfer equation. As a first step in this direction one may describe the radiative losses in the Newtonian cooling approximation, which assumes that a temperature perturbation T_1 is damped on a characteristic timescale τ_R according to

$$\partial_t \frac{T_1}{T_0} + v_{1z} \frac{1}{T_0} \frac{\mathrm{d}T_0}{\mathrm{d}z} + (\gamma - 1) \nabla \cdot \boldsymbol{v}_1 = -\frac{1}{\tau_R} \frac{T_1}{T_0} , \tag{1}$$

where $\boldsymbol{v}_1 = \partial_t \boldsymbol{\xi}$ is the velocity perturbation and the Newtonian cooling time τ_R is given by (Spiegel 1957)

$$\tau_R = \frac{\rho_0 c_V}{16 \chi \sigma_R T_0^3} \left[1 - \left(\frac{\chi}{k} \right) \operatorname{arccot} \left(\frac{\chi}{k} \right) \right]^{-1} . \tag{2}$$

Here ρ_0 is the mass density, χ the mean absorption coefficient per cm, σ_R the Stefan-Boltzmann constant, and k the wavenumber. The term in square brackets increases monotonically from 1 to $+\infty$ as χ/k increases from 0 to $+\infty$.

In the optically thin case, where the wavelength of the perturbation is small relative to the photon mean free path (i.e. $\chi/k \ll 1$), the wavenumber dependence may be neglected and τ_R ranges between $\simeq 0.5$ s at $z = 0$ ($\tau_{5000} = 1$) and $\simeq 300$ s at a height of +500 km ($\tau_{5000} = 3 \cdot 10^{-4}$). For waves whose wavelength is not small compared to the photon mean free path (i.e. for "optically thick" perturbations) the wavenumber correction generally increases τ_R. At $\tau_{5000} = 1$, a wave with $\lambda_x = 700$ km – a typical value in our calculations – gives $\chi/k_x = 2.9$, and τ_R is increased by a factor of 27. The slow mode (with period 190 s $\gg \tau_R$ at this λ_x) lives close to the interface at $\tau_{5000} = 1$ and will be close to 'isothermal'. At one pressure scale height above $\tau_{5000} = 1$, where the first harmonic mode (period 90 s) typically reaches its largest amplitudes, $\tau_R \simeq 9$ s and the correction factor for $\lambda_x = 700$ km is 1.3, so that it is also expected

to lie closer to the isothermal case than to the adiabatic. Hence, Newtonian cooling should greatly affect the wave modes under consideration, in spite of their comparatively long wavelengths. It is therefore important to include these dissipative effects in our current model.

In the following we will assume a constant τ_R. This choice is not ideal, but necessary to allow an analytical treatment. An attempt to relax this condition has been made by Stix (1970), who considered non-magnetic oscillations in a three-layered atmospheric model with piece-wise constant Newtonian cooling time. A similar procedure could be tried in our context, but is outside the scope of this paper.

In the case of an isothermal equilibrium atmosphere the effects of Newtonian cooling may be included by a simple transformation of the adiabatic exponent $\gamma \rightarrow \hat{\gamma} = (1 + i\omega\tau_R\gamma)/(1 + i\omega\tau_R)$ (Bünte & Bogdan 1994), where the time dependence of the oscillation is given by $\exp(+i\omega t)$. The theoretical description of a radiatively damped wave remains formally identical to the adiabatic case treated by Miles et al. (1992), except for the appearance of the complex, frequency-dependent $\hat{\gamma}$ and $\hat{C}_S^2 = \hat{\gamma}p/\rho$ in place of γ and the adiabatic sound speed $C_S^2 = \gamma p/\rho$, respectively. The corresponding dispersion relation thus becomes a complex equation in ω, whose imaginary part reflects the fact that Newtonian cooling leads to temporal decay of the oscillations. The temperature perturbation may be written as

$$T_1 = \frac{i(\hat{\gamma}-1)T_0}{\omega\left(k_x^2\hat{C}_S^2 - \omega^2\right)}\left(k_x^2 g - \omega^2\frac{\mathrm{d}}{\mathrm{d}z}\right)v_{1z}\,, \qquad (3)$$

where k_x is the horizontal wave-number and g the gravitational acceleration. In the limit $\omega\tau_R \rightarrow \infty$ we have $\hat{\gamma} \rightarrow \gamma$ and recover the adiabatic temperature perturbation used in Sect. 2, while in the case $\omega\tau_R \rightarrow 0$, we have $\hat{\gamma} \rightarrow 1$, and the temperature perturbation vanishes. In this limit the magneto-atmospheric surface waves again propagate without decaying since the frequency eigenvalues are again real. The phase relations between the various perturbations are the same as in the adiabatic case (see Appendix A of Bünte et al. 1993).

3.2. Isothermal MHD waves

Let us consider now the extreme case $\tau_R = 0$. As before the free parameters of our model are the height of the horizontal interface and the constant magnetic field strength. Placing the lower boundary of the penumbra at $\tau_{5000} = 1$ and assuming a field strength of 1000 G we obtain $C_i/C_e = 0.835$ and $V_A(0)/C_e = 0.816$, where C_i and C_e are the constant sound speeds in the magnetic and non-magnetic layers, respectively[2], and $V_A(0)$ is the Alfvén speed at the interface.

The corresponding dispersion diagram is shown in Fig. 3. There are again two types of modes, one with small phase velocity (the slow mode), the other with large phase velocity (the trapped harmonic modes). The lowest dot-dashed line gives the limit to which the slow mode develops in the case of zero gravity (Miles et al. 1992). Due to the instantaneous temperature smoothing for $\tau_R = 0$, propagating low-frequency gravity-dominated oscillations vanish completely (Souffrin 1966; Mihalas & Mihalas 1984; Bünte & Bogdan 1994). This corresponds to the disappearance of the R_1-curve in the dispersion diagram. Oscillatory modes are restricted to the region above the R_2-curve (the dotted line).

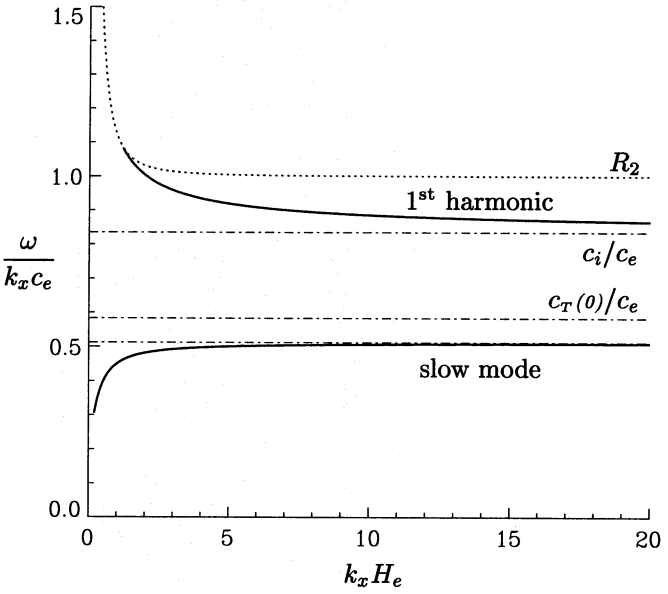

Fig. 3. Non-dimensional dispersion diagram $Y = \omega/(k_x C_e)$ vs. $X = H_e k_x$ for isothermal magneto-atmospheric surface waves ($\tau_R = 0$). In this diagram $C_i/C_e = 0.835$, $V_A(0)/C_e = 0.816$, $C_T(0) = C_i V_A(0)/\sqrt{C_i^2 + V_A(0)^2} = 0.584\,C_e$, and $\gamma = 1$

In view of the radiative transfer calculations carried out in the following section we note that in the case $\tau_R \rightarrow 0$ the temperature perturbation T_1 vanishes also in the case of a non-isothermal equilibrium atmosphere, as may be seen from Eq. (1). Hence, the temperature as a function of geometrical height is left untouched by an isothermal wave and it is the correlation of pressure and density fluctuations with the horizontal velocity component that determines the spectral signature of the waves.

Note that in a radiative transfer calculation temperature fluctuations nevertheless arise along iso-log τ-contours, as shown schematically in Fig. 4. While isothermal waves do not create any temperature fluctuations by themselves, the pressure and density perturbations lift the iso-log τ-contours (thick wavy line) into higher, cooler regions above wave crests and shift them down into hotter domains in wave troughs. This leads to a temperature-velocity correlation along iso-log τ-contours which is exactly opposite to, but less pronounced than in the case of an adiabatic wave. Note that this correlation is not due to any inconsistency in the computation of the wave modes, but that it is a higher order effect arising from first order pressure and density perturbations in a consistent radiative transfer calculation.

[2] Following Bünte et al. (1993) we give C_i and C_e the values of the undisturbed atmosphere just above and just below the interface, respectively.

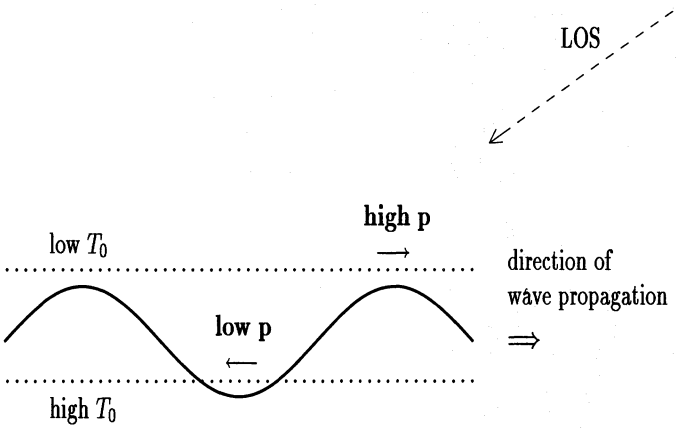

Fig. 4. Schematic drawing of an isothermal wave propagating horizontally to the right. The correlated pressure and horizontal velocity perturbations are indicated. The temperature stratification of the equilibrium atmosphere gives rise to a temperature–velocity correlation along the wavy iso-log τ-contour

4. The spectral signature of waves subject to strong radiative diffusion

To explore the spectroscopic effects of the pressure-velocity correlation of radiatively damped surface and trapped body waves we consider the case $\tau_R = 0$ described in the preceding section.

Figure 5 shows the synthetic profiles of the three iron lines Fe I 5250.2 Å, 5576.1 Å, and 15648.5 Å. They have been computed in the presence of the first harmonic mode with a wavelength of 400 km and period $P = 63$ s for $\tau_R = 0$. As in Fig. 2 we have chosen $\theta = 70°$. The maximum LOS-velocity is 1.8 km s^{-1}. In contrast to adiabatic waves, strongly damped "isothermal" waves shift all three profiles towards the blue when travelling *towards* the observer.

In the following we examine the physical origin of this behaviour in greater detail. We show that the above neutral lines are dominated by the wave-induced density fluctuations (leading to the blue-shifts seen in Fig. 5), while the behaviour of ionized lines, such as Fe II 5325.6 Å, is determined by the temperature-velocity correlation along iso-log(τ) surfaces (induced by the waves as described in the previous Sect.).

4.1. Physical origin of the wave signature

The wave-induced fluctuations in the gas pressure p act on the line profiles in multiple ways, firstly over the total number density of particles, secondly over the ionization balance (via the electron density in the Saha equation), thirdly over the continuum opacity, and fourthly over the damping constant, dominated by Van der Waals damping.

The influence on the damping constant is only important for strong lines with prominent damping wings: the strength of the damping wings increases with increasing pressure due to the increasing number of collisions. This effect plays a minor role and will be neglected in the following discussion. It should be noted, however, that it is included in our fully self-consistent radiative transfer calculations.

The waves affect the line profiles mainly through fluctuations in total particle density and electron pressure and indirectly (i.e. in a radiative transfer calculation) through temperature fluctuations along iso-log τ surfaces (see the last paragraph in Sect. 3.2). The latter two quantities influence the ionization equilibrium. All together they lead to fluctuations in the number densities N^0 and N^+ of neutral and ionized Fe atoms, respectively. The regions where these are increased dominate the emerging line profiles whose shifts arise from the predominant local particle motions. To understand the spectral signature of the waves we must, therefore, consider the reaction of N^0 and N^+ to the wave perturbations.

According to the Saha equation the number densities N^0 and N^+ are given by

$$N^0 = \frac{p_e/f(T)}{1+p_e/f(T)} N \quad \text{and} \quad N^+ = \frac{1}{1+p_e/f(T)} N\,, \tag{4}$$

where $N = N^0 + N^+$ is the total number density of iron particles, p_e is the electron pressure, and $f(T)$ is given by

$$f(T) = \frac{U^+}{U^0} \frac{2\,(2\pi m_e)^{3/2}}{h^3} (k_B T)^{5/2}\, e^{-\chi_i/k_B T}\,, \tag{5}$$

where U^0 and U^+ are the partition functions of Fe^0 and Fe$^+$, k_B is Boltzmann's constant, h the Planck constant, m_e the electron mass, and $\chi_i = 7.87$ eV the ionization potential of Fe^0.

Now consider the fluctuations $\delta N^+/N^+$ and $\delta N^0/N^0$ induced by a wave on an iso-log τ surface in an atmosphere which is stratified in temperature. In our radiative transfer calculations we determine these fluctuations consistently from the perturbed atmosphere. In order to disentangle the combined influence of the various physical parameters (fluctuations in total particle density N, electron pressure p_e, and temperature T, which by themselves are not independent of each other) it is instructive to consider the linearized expressions of $\delta N^0/N^0$ and $\delta N^+/N^+$ obtained from Eqs. (4) & (5):

$$\frac{\delta N^0}{N^0} = \frac{\delta N}{N} + \frac{N^+}{N}\frac{\delta p_e}{p_e} - \frac{N^+}{N}\left(\frac{5}{2} + \frac{\chi_i}{k_B T}\right)\frac{\delta T}{T}\,, \tag{6}$$

$$\frac{\delta N^+}{N^+} = \frac{\delta N}{N} - \frac{N^0}{N}\frac{\delta p_e}{p_e} + \frac{N^0}{N}\left(\frac{5}{2} + \frac{\chi_i}{k_B T}\right)\frac{\delta T}{T}\,, \tag{7}$$

where δN, δp_e, and δT are the differences in number density, electron pressure, and temperature between perturbed and unperturbed atmosphere *at fixed optical depth*[3]. In the presence of the wave a formerly horizontal iso-log τ surface is distorted into a wavy surface with troughs and crests at different heights (and temperatures) in the atmosphere. Hence, the above fluctuations generally differ from the *local* wave perturbations which refer to a constant height in the atmosphere.

[3] The linearized expressions fare quite well (with errors less than 10 %) when compared with the self-consistently calculated values of $\delta N^0/N^0$ and $\delta N^+/N^+$ (see Fig. 6)

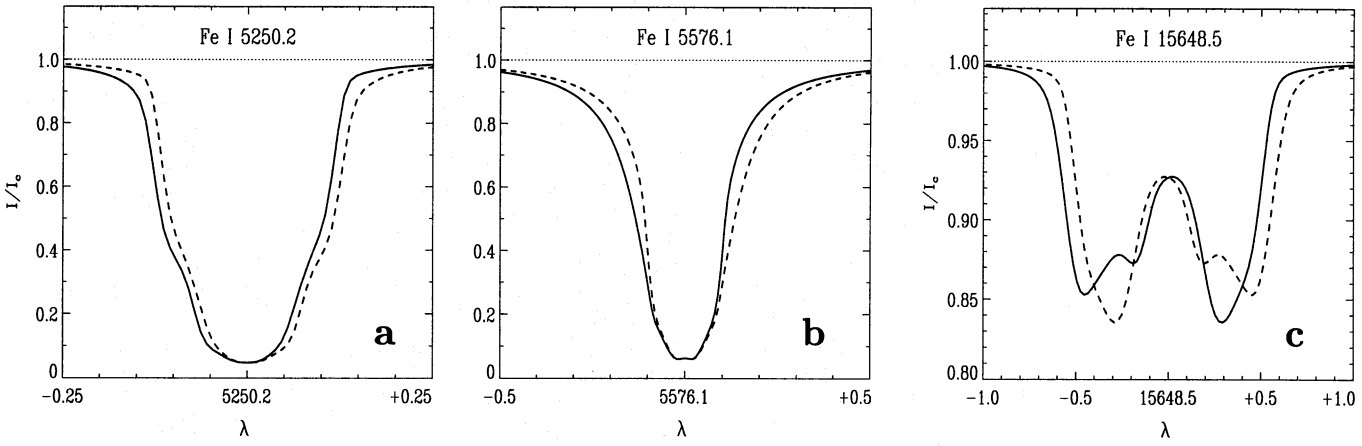

Fig. 5a–c. Synthetic line profiles of **a** Fe I 5250.2 Å, **b** 5576.1 Å, and **c** 15648.5 Å for observations of the isothermal ($\tau_R = 0$) fast mode ($\lambda_x = 400$ km, $P = 63$ s; $\hat{v}_{1z}(0) = 1.5$ km s^{-1}) close to the limb ($\theta = 70°$; solid); the dashed lines represent the mirrored profile in each case. The profiles show systematic blue-shifts and asymmetries due to the pressure-velocity correlation of the isothermal wave. In contrast, at disc centre they are symmetric

In the presence of the wave the total particle density N generally decreases in troughs and increases in crests, and is only slightly counteracted by the density stratification. As one would expect, temperature and electron pressure show the opposite behaviour, i.e. they are increased in the troughs and decreased in the crests[4]. For the wave considered in Fig. 5 theses fluctuations vary across one wavelength between -30% and $+20\%$ for N, between $+5\%$ and -3% for T, and between $+30\%$ and -10% for p_e at $\log\tau = -2$. Note that the temperature fluctuations are small, in particular in comparison with the adiabatic case in which they lie between -10% and $+20\%$.

For comparison, at constant height 156 km above the penumbral boundary (corresponding to $\log\tau = -2$) the local changes in N (between $\mp 40\%$) and p_e (between -30% and $+25\%$) are in phase, and the temperature perturbations are strictly zero.

Before considering in the following section the wave signature resulting from the various wave perturbations we note that the coefficients of the perturbation terms in Eqs. (6) & (7) differ quite drastically. At $\log\tau = -2$ we have $N^0/N = 0.93$ and $N^+/N = 0.07$, while $\chi_i/(k_B T) = 18.3/T[5000\,\mathrm{K}] = 24$[5]. Due to the smallness of the temperature fluctuations the temperature sensitivity of a spectral line will not have any impact on the spectral signature of the wave. At this temperature the magnitude of the weight of $\delta T/T$, however, indicates that temperature fluctuations will play an important role for the lines of ionized species by shifting the ionization equilibrium.

4.2. *The wave signature in Fe* I *and Fe* II *lines*

In Fig. 6 we have plotted $\delta N^0/N^0$ (upper panel) and $\delta N^+/N^+$ (lower panel) arising from the wave considered in Fig. 5 at $\log\tau = -2$ (thick solid lines). Note that $\delta N^0/N^0$ and $\delta N^+/N^+$ show exactly the opposite behaviour in wave troughs and crests. This is illuminated by the linear approximations from Eqs. (6) & (7) which are plotted as the dot-dashed lines along with the respective contributions (the terms on the r.h.s.) from $\delta N/N$ (dashed), $\delta p_e/p_e$ (dotted), and $\delta T/T$ (triple dot-dashed). Obviously, $\delta N^0/N^0$ is dominated by the fluctuations in total particle density, while $\delta N^+/N^+$ is determined by the temperature fluctuations along the iso-$\log\tau$ surface whose contribution counteracts and over-compensates all the other contributions.

We are hence led to the conclusion that neutral lines are dominated by the high density crests where the particles move towards the observer (cf. Fig. 1). Due to the smallness of the temperature fluctuations this density effect covers the different temperature sensitivities of the Fe I lines, leading to line-independent blue-shifts (Fig. 5). On the other hand, Fe II lines due to their high sensitivity even to small temperature changes, are dominated by the slightly hotter low density troughs. Since there the particles are moving away from the observer (Fig. 4) this should result in a red-shift of Fe II lines.

This expectation is confirmed by a detailed computation. Figure 7 shows the line profile of Fe II 5325.6 Å, which has been computed from exactly the same model as used in the computations for Fig. 5. The prominent increase of N^+ in the troughs of the waves leads to a net red-shift of the line profile, exactly opposite to the Fe I lines. Thus, since the Evershed effect is observed in Fe I&II lines simultaneously with the same sign (Stellmacher & Wiehr 1980), also isothermal waves fail to provide a coherent alternative explanation of the observed line shifts and asymmetries.

4.3. *Isothermal atmospheres*

While the results shown in Figs. 5 and 7 are in line with our above interpretation, they seem to contradict Maltby & Eriksen (1967), who in the presence of pressure waves (with no intrinsic temperature fluctuations) obtained results independent of the

[4] Well below the line forming layers, close to the penumbral boundary, this behaviour is reverted due to the large gradients that characterize the transition to the underlying convection zone

[5] Fe is mainly neutral since we consider a penumbral model which is substantially cooler than the quite sun atmosphere

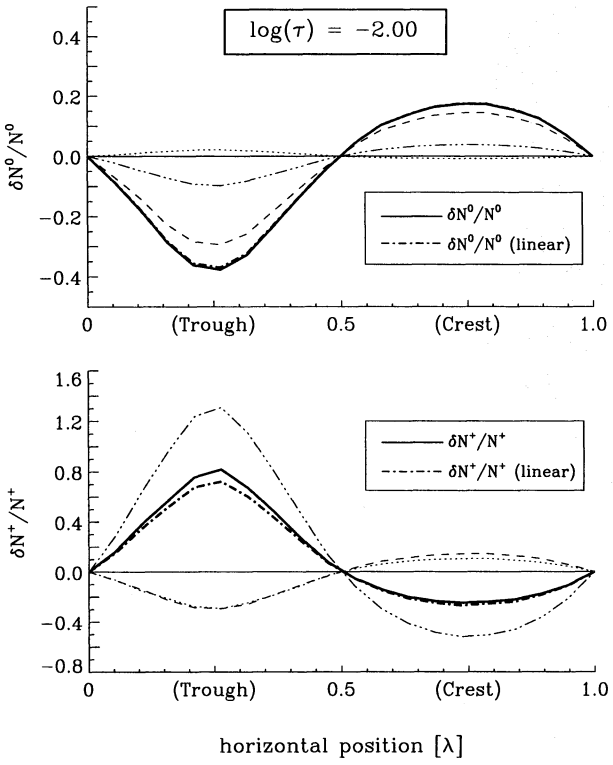

Fig. 6. Fluctuations in number densities (solid lines): $\delta N^0/N^0$ (upper panel) and $\delta N^+/N^+$ (lower panel) over one wavelength of the isothermal fast mode (with wavelength λ = 400 km) at constant $\log\tau = -2$. The respective linear approximations from Eqs. (6) & (7) are shown as the dot-dashed lines along with the various contributions by $\delta N/N$ (dashed), $\delta p_e/p_e$ (dotted), and $\delta T/T$ (triple dot-dashed). In the case of neutrals it is the crest-, in the case of ions the trough-contributions that dominate

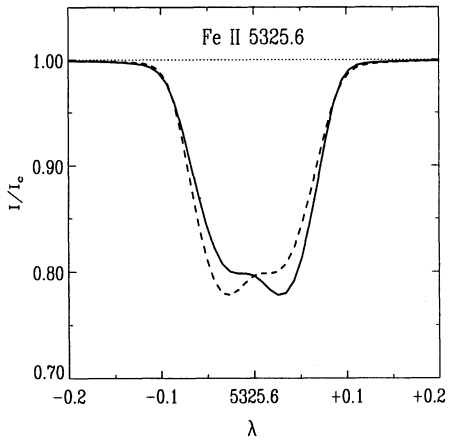

Fig. 7. Synthetic line profile of Fe II 5325.6 Å calculated for the same model that underlies Fig. 5, i.e. in the presence of the isothermal (τ_R = 0) fast mode close to the limb (θ = 70°; solid); the dashed line represents the mirrored profile. The red-shift of the profile is opposite to the blue-shifts exhibited by the Fe I lines (Fig. 5)

ionization state of the atoms. This, however, is a direct consequence of their assumption of a truly isothermal atmosphere. In the absence of any temperature fluctuations, i.e. $\delta T \equiv 0$ in Eqs. (6) & (7), $\delta N^0/N^0$ and $\delta N^+/N^+$ show the same qualitative behaviour in the line forming layers. This is due to the dominance of the density fluctuations over those in electron pressure (cf. Sect. 4.1). Hence, Fe I and Fe II lines should in fact always behave similarly in an atmosphere that remains isothermal at a given $\log\tau$ over a full wave period.

Finally we note that, in contrast to the temperature, the electron density enters only linearly into the Saha-Boltzmann equilibrium. Similarly, opacity fluctuations affect the continuum intensity far less efficiently than changes in the Planck function, which depends only on the temperature. Hence, it is not surprising that in order to obtain a measurable effect the vertical velocity amplitude had to be increased by a factor of 2 as compared to the adiabatic calculations in Sect. 2. Also, in the presence of the slow mode the effects of the waves on the line profiles are smaller.

5. Discussion and conclusions

We have reconsidered the surface wave model of the Evershed effect suggested recently by Bünte et al. (1993). Their promising results for the neutral iron line Fe I 5250.2 Å have motivated the present more detailed analysis of the complex influence of magneto-atmospheric waves on the formation of spectral lines. We have extended their analysis by considering the effects of both adiabatic and radiatively damped magneto-atmospheric waves on several spectral lines.

Adiabatic waves cause large temperature fluctuations that are correlated with the horizontal velocity. We have shown in Sect. 2 that the net line shift, produced for observations close to the limb, depends on the interplay between phase dependent changes in continuum intensity and line strength variations (produced by variations in the ionization and excitation equilibria). Since the latter depend on the temperature sensitivity of a spectral line, adiabatic waves cannot systematically reproduce the spectral signature of the Evershed effect that is observed (e.g. Ichimoto 1987).

Wave motions in a radiatively dominated medium like the solar photosphere should suffer severe radiative damping. In a second step we have, therefore, extended the surface wave model by including the effects of radiative damping in the simple Newtonian cooling approximation (Sect. 3). In the case of perfect radiative dissipation the temperature fluctuations are so small that the formation of the line profiles is no longer dominated by the interplay between changes in continuum intensity and variations in excitation equilibrium. We rather find that the spectral lines from neutrals are dominated by the wave-induced changes in density and hence by the wave crest contributions, while those of ions are determined by the small temperature fluctuations along iso-$\log\tau$ surfaces and hence by the trough contributions (Sect. 4). Consequently, Fe II lines show the opposite behaviour to Fe I lines, in contrast to what is observed (Stellmacher & Wiehr 1980).

The origin of this different behaviour lies in the temperature stratification of the equilibrium atmosphere. In an isothermal

atmosphere permeated by an isothermal wave, as considered by Maltby & Eriksen (1967), neutral and ionized species behave similarly. This explains the difference between the conclusions reached by Maltby & Eriksen (1967) and us.

The arguments against magneto-atmospheric surface waves presented here are just as applicable to other types of compressible waves and, therefore, question linear wave models of the Evershed effect in general.

The model we have adopted is rather crude, and has a number of shortcomings. Firstly, we have assumed an isothermal background atmosphere for the computations of the surface wave eigenmodes which is a questionable assumption, in particular in the photosphere.

Secondly, the Newtonian cooling approximation is an oversimplification of the radiative dissipation to be expected in these layers. On the one hand, radiative diffusion will tend to smear out temperature fluctuations along iso-log τ-contours. In our model, these temperature changes arise as a consequence of the linear wave perturbations and are not further affected by Newtonian cooling which itself represents only a linear approximation to radiative diffusion. This calls for non-linear computations of waves in a radiating medium. On the other hand, although radiative dissipation will be efficient in photospheric layers the wave-induced temperature perturbations will not be destroyed completely, in particular in the higher line-forming regions. For the purposes of radiative transfer such waves might come closest to truly isothermal waves with constant temperature along iso-log τ-contours. Such a wave would produce shifts of equal sign in all spectral lines. However, the set of parameters in our model would have to be fine-tuned with high precision to achieve such a cancellation of the various temperature fluctuations. We therefore consider this an unlikely possibility and have not followed it further in this contribution.

Thirdly, the wave amplitudes needed to produce measurable shifts of the order of 1 $\mathrm{km\,s^{-1}}$ are of considerable magnitude (e.g. $|p_1| \simeq 0.67 p_0$!) and all but small compared to the equilibrium values, suggesting that we are stretching the limits of linear wave theory: the effects of non-linearity, e.g. non-linear pulsations, should be explored.

In summary, considering that both adiabatic and isothermal waves have serious difficulty accounting for the observed Evershed effect in photospheric penumbral lines, we conclude that linear wave models in general, and the surface wave model in particular, do not provide a convincing explanation of the Evershed phenomenon.

Unfortunately, the demise of the linear wave model brings us no closer to a convincing theory of the Evershed effect. We believe that it would greatly enhance the case for remaining models if they could be shown to reproduce the observed line shifts and asymmetries. A first step in this direction has been taken by Degenhardt (1993), but much work remains to be done.

Acknowledgements. We thank K. Jahn and H.U. Schmidt for lively discussions on this subject. M.B. wishes to acknowledge financial support by the Swiss National Science Foundation under grant No. 20-31 289.91.

References

Bünte, M.: 1993, Ph.D. Thesis, ETH Zürich, No. 10 357
Bünte, M., Bogdan, T.J.: 1994, A&A **283**, 642
Bünte, M., Solanki, S.K.: 1994, in *Solar magnetic fields*, M. Schüssler, W. Schmidt (eds.), Cambridge University Press, Cambridge, p. 179
Bünte, M., Darconza, G., Solanki, S.K.: 1993, A&A **274**, 478
Darconza, G.: 1992, *Diplomarbeit*, ETH Zürich
Degenhardt, D.: 1993, A&A **277**, 235
Ding, M.D., Fang, C.: 1989, A&A **225**, 204
Eriksen, G., Maltby, P.: 1967, ApJ **148**, 833
Evershed, J.: 1909, MNRAS **69**, 454
Ichimoto, K.: 1987, Publ. Astron. Soc. Japan **39**, 329
Lamb, S.A.: 1975, MNRAS **172**, 205
Maltby, P., Eriksen, G.: 1967, Solar Phys. **2**, 249
Mihalas, D., Mihalas, B.W.: 1984, *Foundations of Radiation Hydrodynamics*, Oxford University Press, New York
Miles, A.J., Allen, H.R., Roberts, B.: 1992, Solar Phys. **141**, 235
Rimmele, Th.: 1993, Ph.D. Thesis, Albert-Ludwigs-Universität, Freiburg i. Br.
Schröter, E.H.: 1965, Z. Astrophys. **62**, 228
Schröter, E.H., Kentischer, T., Münzer, H.: 1989, in *High Spatial Resolution Solar Observations*, O. von der Lühe (ed.), National Solar Obs., Sunspot, NM, p. 229
Solanki, S.K., Montavon, C.A.P.: 1993, A&A **275**, 283
Solanki, S.K., Montavon, C.A.P., Livingston, W.: 1992, in *The Magnetic and Velocity Fields of Solar Active Regions*, H. Zirin (ed.), PASPC, IAU Coll. 141, p. 52
Solanki, S.K., Montavon, C.A.P., Livingston, W.: 1994, A&A **283**, 221
Souffrin, P.: 1966, Ann. Astrophys. **29**, 55
Spiegel, E.A.: 1957, ApJ **126**, 202
Spruit, H.C.: 1977, Ph.D. Thesis, Univ. Utrecht
Stellmacher, G., Wiehr, E.: 1980, A&A **82**, 157
Stix, M.: 1970, A&A **4**, 189

This article was processed by the author using Springer-Verlag TEX A&A macro package 1992.